A Novel 24-Pulse Diode Rectifier with an Auxiliary Single-Phase Full-Wave Rectifier at DC Side

Shiyan Yang, Jingfang Wang, and Wei Yang, *Member, IEEE*

***Abstract*—A simple and robust 24-pulse diode rectifier for low-voltage and high-current applications is proposed in this paper. The proposed 24-pulse diode rectifier consists of a conventional four-star 12-pulse diode rectifier and an auxiliary single-phase full-wave rectifier (ASFR) installed at dc side. The low-power (3.4%Po) ASFR extracts two rectangular currents from the modified second-stage interphase transformer and injects a square current into the output of the rectifier system. This modification extends the conventional four-star 12-pulse operation to 24-pulse operation. The proposed 24-pulse rectifier draws near sinusoidal input line currents with the absence of 5th, 7th, 11th, 13th, 17th, and 19th harmonics. The average value of current through the ASFR has only 1.7% of load current, which means the current rating and conduction losses of ASFR are very small. The proposed scheme has low-diode conduction losses, and it is more suitable for low-voltage and large-current applications. Since only an additional ASFR is needed, the proposed scheme is low cost and simple to implement. The detailed analysis for the proposed rectifier is presented, and experimental results are provided to verify the proposed concept.**

***Index Terms*—Harmonics, interphase transformer, single-phase full-wave rectifier, 24-pulse rectifier.**

I. Introduction

THE conventional four-star 12-pulse diode rectifier, which presents lower diode conduction losses than the 12-pulse diode bridge rectifier, is commonly used in low-voltage and high-current applications such as electrochemical, electrowinning, dc arc furnaces, plasma torches, etc. [1]–[3]. The four-star 12-pulse diode rectifier not only doubles the output power of the six-pulse rectifier, but also offset the fifth and seventh harmonics produced by each of the six-pulse rectifier. Although it can cancel the fifth and seventh harmonics in the input line current, the total harmonic distortion (THD) of the current is still high.

To lower the input line current harmonics, many methods have been proposed [4]–[20]. Among them, increasing the number of pulses of diode rectifiers is one of the most effective methods [9]–[20]. In [9]–[12], several 24-pulse diode rectifiers with multiphase transformers are presented. These 24-pulse diode rectifiers draw near sinusoidal input line currents with the 5th, 7th, 11th, 13th, 17th, and 19th harmonics eliminated from the input line currents. However, the structure of multiphase transformers is complicated, and the number of diodes is twice over the conventional 12-pulse diode rectifier, which adds to the complexity, cost, and size. To increase the number of pulses with slight complexity in hardware, a dc ripple reinjection method has been used to lower the input line current harmonics [13]–[15]. In [13], a dc ripple reinjection circuit for pulse doubling is proposed. It applies a set of passive auxiliary circuit to double the number of pulses. However, the number of elements is still high, the volt-ampere ratings of the current-injection device are large, and the input and output are nonisolated. To double the number of pulses with the least components, the tapped interphase transformers (TIPTs) with two additional diodes are proposed to extend the conventional 12-pulse operation to 24-pulse operation [16]–[20]. These 24-pulse diode rectifiers with TIPT draw near sinusoidal input line currents with the least number of additional components. However, the two additional diodes linked with the taps of the TIPT are in series with the load; the total currents through two additional diodes are 100% load current. Diodes conduction losses of these 24-pulse rectifiers with TIPT are the triple of diode conduction losses of the conventional four-star 12-pulse rectifier. Diode conduction losses of the 24-pulse rectifier with TIPT are serious, thus making these schemes nonapplicable for low-voltage and high-current applications.

In this paper, a novel 24-pulse diode rectifier, which has simple circuit configuration and low diode conduction losses, for low-voltage and high-current applications is proposed. Fig. 1 shows the proposed 24-pulse diode rectifier. It consists of a conventional four-star 12-pulse diode rectifier and an auxiliary single-phase full-wave rectifier (ASFR). The proposed scheme has the following advantages.

1) The proposed 24-pulse rectifier is totally passive and has the least number of components count, making it robust and simple to implement.
2) A low-power (3.4% Po) ASFR is enough to extend the conventional four-star 12-pulse operation to 24-pulse operation.
3) The output of ASFR is connected in parallel with the load, which results in very small current (1.7%Id) through the ASFR. The current rating and conduction losses of the ASFR are very low, and the ASFR can be configured with low cost. Compared with other 24-pulse diode rectifiers with auxiliary pulse doubling circuit (TIPTs) [16]–[20], the proposed scheme does not have diodes in series with the load, which avoids unwanted voltage drops in the path of the main load

Manuscript received December 31, 2015; revised February 29, 2016; accepted April 14, 2016. Date of publication April 28, 2016; date of current version December 9, 2016. Recommended for publication by Associate Editor B. Singh.

The authors are with the School of Electrical Engineering and Automation, Harbin Institute of Technology, Harbin 150006, China (e-mail: syyang@hit.edu.cn; wjfyjs550@126.com; yangv@hit.edu.cn).

Color versions of one or more of the figures in this paper are available online at http://ieeexplore.ieee.org.

Digital Object Identifier 10.1109/TPEL.2016.2560200

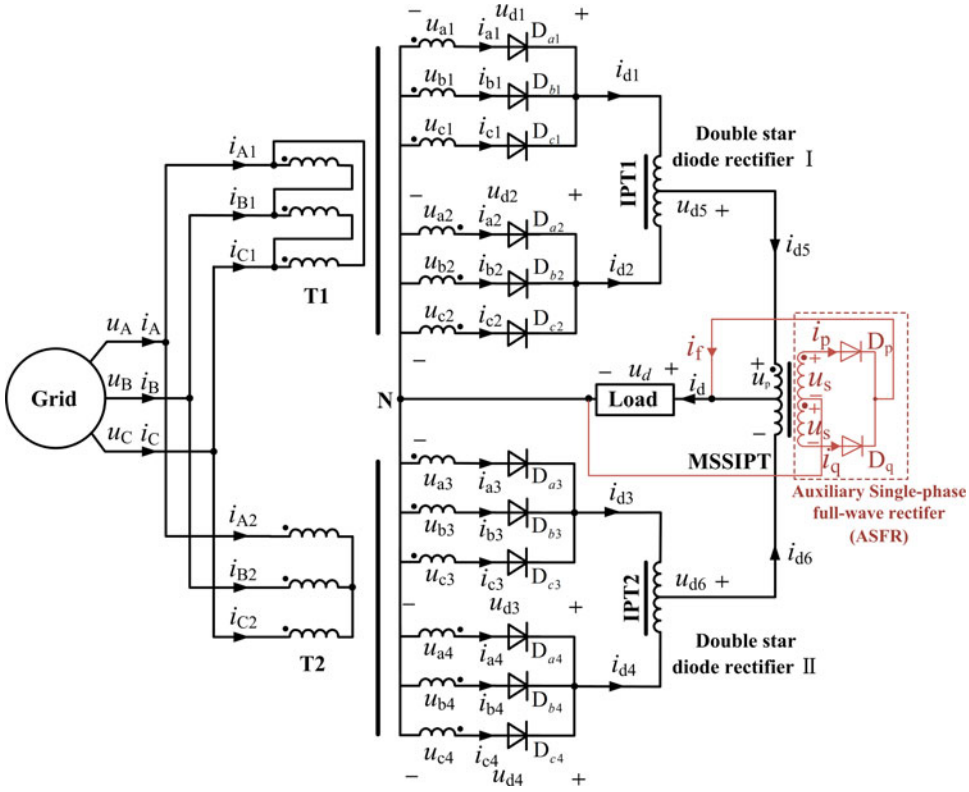

Fig. 1. Circuit configuration of the proposed 24-pulse rectifier.

current and has lower diode conduction losses. The proposed method is more suitable for low-voltage and high-current applications.

4) In the event the ASFR malfunctions, the proposed rectifier can operate as a conventional four-star 12-pulse diode rectifier. The fifth and seventh harmonics are still eliminated completely.

The detailed analysis of the proposed 24-pulse diode rectifier is discussed in the following sections.

II. Circuit Configuration and Operation Mode

A. Circuit Configuration

Fig. 1 shows the proposed 24-pulse diode rectifier. It is identical to the conventional four-star 12-pulse rectifier, with the exception of a modified second-stage interphase transformer (MSSIPT) and the ASFR connected in parallel with the MSSIPT. Compared with the conventional second-stage interphase transformer, the MSSIPT has an additional winding with a center tap. The additional winding with a center tap is used to install the low-power ASFR. The ASFR extracts two rectangular currents from the MSSIPT and injects a square current into the output of the proposed rectifier. This modification extends the conventional four-star 12-pulse rectifier to 24-pulse rectifier. The primary windings of two double-star transformers are configured in delta-wye-wye and wye-wye-wye connection, respectively. By using this connection, two double-star transformers provide 30° phase shift at the secondary side.

To facilitate the analysis in the next sections, the following assumptions for Fig. 1 are given below.

1) The proposed rectifier is supplied by a balanced undistorted three-phase voltage system, specified by input phase voltages

$$\begin{cases} u_A = U_G \sin(\omega t) \\ u_B = U_G \sin(\omega t - 2\pi/3) \\ u_C = U_G \sin(\omega t + 2\pi/3) \end{cases} \tag{1}$$

where U_G is the amplitude of the input phase voltage.

2) Turns ratio between the primary windings and secondary windings in two double-star transformers with delta-wye-wye and wye-wye-wye connection is $\sqrt{3}k:1$ and $k:1$, respectively.

3) Turns ratio of the primary and the half secondary windings of the MSSIPT is

$$N_p : N_s = 1 : m. \tag{2}$$

4) The load, shown in Fig. 1, is a large inductance loading and the load current i_d can be viewed as a constant I_d.

5) The leakage inductances and resistances of double-star transformers and interphase transformer are neglected.

B. Necessary Condition

In Fig. 1, if the maximum value of the ASFR input voltage $|u_s|$ is less than the minimum value of load voltage u_d, the diodes of ASFR are reverse-biased and the ASFR does not work. The proposed rectifier operates as a conventional four-star 12-pulse

diode rectifier. Therefore, to ensure the ASFR works normally, the maximum value of input voltage $|u_s|$ should be higher than the minimum value of load voltage u_d. Since the voltage $|u_s|$ is determined by the turns ratio of the MSSIPT, it means that the turns ratio of the MSSIPT should be large enough to ensure the ASFR works normally. In this section, the boundary turns ratio when the ASFR can work will be discussed.

When the ASFR does not work, the proposed rectifier operates as a conventional four-star 12-pulse diode rectifier. In this case, four three-phase half-wave rectifier output voltages $u_{d1},\ u_{d2},\ u_{d3}$, and u_{d4} can be expressed as

$$\begin{cases} u_{d1} = \max(u_{a1}, u_{b1}, u_{c1}) \\ u_{d2} = \max(u_{a2}, u_{b2}, u_{c2}) \\ u_{d3} = \max(u_{a3}, u_{b3}, u_{c3}) \\ u_{d4} = \max(u_{a4}, u_{b4}, u_{c4}) \end{cases} \tag{3}$$

where $u_{a1},\ u_{b1},\ u_{c1},\ u_{a2},\ u_{b2},\ u_{c2},\ u_{a3},\ u_{b3},\ u_{c3},\ u_{a4},\ u_{b4},$ and u_{c4} are output voltages of secondary sides of two double-star transformers, and they can be expressed as

$$\begin{cases} u_{a1} = \dfrac{\sqrt{3}U_G}{k}\sin(\omega t + \pi/6) \\ u_{b1} = \dfrac{\sqrt{3}U_G}{k}\sin(\omega t - \pi/2) \\ u_{c1} = \dfrac{\sqrt{3}U_G}{k}\sin(\omega t + 5\pi/6) \\ u_{a2} = \dfrac{\sqrt{3}U_G}{k}\sin(\omega t - 5\pi/6) \\ u_{b2} = \dfrac{\sqrt{3}U_G}{k}\sin(\omega t + \pi/2) \\ u_{c2} = \dfrac{\sqrt{3}U_G}{k}\sin(\omega t - \pi/6) \end{cases} \tag{4}$$

$$\begin{cases} u_{a3} = \dfrac{\sqrt{3}U_G}{k}\sin(\omega t) \\ u_{b3} = \dfrac{\sqrt{3}U_G}{k}\sin(\omega t - 2\pi/3) \\ u_{c3} = \dfrac{\sqrt{3}U_G}{k}\sin(\omega t + 2\pi/3) \\ u_{a4} = \dfrac{\sqrt{3}U_G}{k}\sin(\omega t - \pi) \\ u_{b4} = \dfrac{\sqrt{3}U_G}{k}\sin(\omega t + \pi/3) \\ u_{c4} = \dfrac{\sqrt{3}U_G}{k}\sin(\omega t - \pi/3). \end{cases} \tag{5}$$

The output voltages of two double-star rectifiers are

$$\begin{cases} u_{d5} = \dfrac{u_{d1} + u_{d2}}{2} \\ u_{d6} = \dfrac{u_{d3} + u_{d4}}{2}. \end{cases} \tag{6}$$

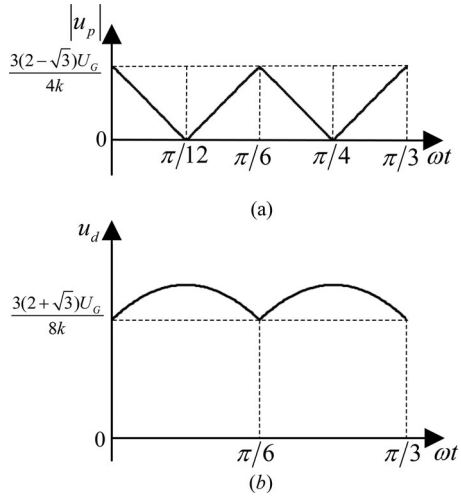

Fig. 2. Voltage $|u_p|$ and load voltage u_d. (a) Voltage $|u_p|$. (b) Voltage u_d.

The voltage across the primary winding of the MSSIPT is

$$u_p = u_{d5} - u_{d6} = \frac{u_{d1} + u_{d2} - u_{d3} - u_{d4}}{2}. \tag{7}$$

The load voltage u_d is

$$u_d = \frac{u_{d5} + u_{d6}}{2} = \frac{u_{d1} + u_{d2} + u_{d3} + u_{d4}}{4}. \tag{8}$$

Since the period of voltage u_p is one-sixth of the input phase voltage period, in one of its period ($\omega t \in [0, \pi/3]$), analyzing the relation between the voltage u_p and load voltage u_d is sufficient.

In the interval $\omega t \in [0, \pi/3]$, substituting (3)–(5) into (7), the voltage u_p is obtained as

$$u_p = \begin{cases} -\dfrac{3(\sqrt{6}-\sqrt{2})U_G}{4k}\cos(\omega t + 5\pi/12), & \omega t \in \left[0, \dfrac{\pi}{6}\right] \\ \dfrac{3(\sqrt{6}-\sqrt{2})U_G}{4k}\cos(\omega t + \pi/4), & \omega t \in \left[\dfrac{\pi}{6}, \dfrac{\pi}{3}\right]. \end{cases} \tag{9}$$

The voltage $|u_p|$ is

$$|u_p| = \begin{cases} \dfrac{3(\sqrt{6}-\sqrt{2})U_G}{4k}\cos(\omega t + 5\pi/12), & \omega t \in \left[0, \dfrac{\pi}{12}\right] \\ -\dfrac{3(\sqrt{6}-\sqrt{2})U_G}{4k}\cos(\omega t + 5\pi/12), & \omega t \in \left[\dfrac{\pi}{12}, \dfrac{\pi}{6}\right] \\ \dfrac{3(\sqrt{6}-\sqrt{2})U_G}{4k}\cos(\omega t + \pi/4), & \omega t \in \left[\dfrac{\pi}{6}, \dfrac{\pi}{4}\right] \\ -\dfrac{3(\sqrt{6}-\sqrt{2})U_G}{4k}\cos(\omega t + \pi/4), & \omega t \in \left[\dfrac{\pi}{4}, \dfrac{\pi}{3}\right]. \end{cases} \tag{10}$$

Substituting (3)–(5) into (8), the voltage u_d is expressed as

$$u_d = \begin{cases} \dfrac{3(\sqrt{6}+\sqrt{2})U_G}{8k}\sin(\omega t + 5\pi/12), & \omega t \in \left[0, \dfrac{\pi}{6}\right] \\ \dfrac{3(\sqrt{6}+\sqrt{2})U_G}{8k}\sin(\omega t + \pi/4), & \omega t \in \left[\dfrac{\pi}{6}, \dfrac{\pi}{3}\right]. \end{cases} \tag{11}$$

Fig. 2 shows the voltage $|u_p|$ and u_d. In Fig. 2, it is clear that at $\omega t = 0$, the maximum value of $|u_p|$ is shown to be

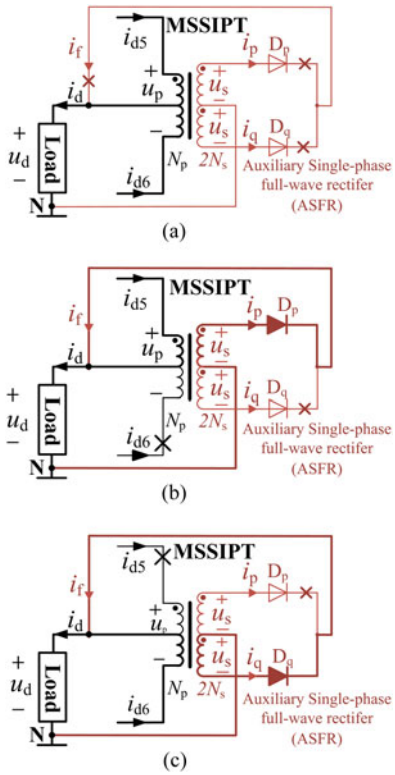

Fig. 3. Operation modes. (a) Z-mode. (b) P-mode. (c) Q-mode.

$3(2-\sqrt{3})U_G/4k$, and the minimum value of u_d is shown to be $3(2+\sqrt{3})U_G/8k$. The minimum value of u_d is 6.96 times the maximum value of $|u_p|$.

The maximum value of $|u_s|$ is obtained as

$$|u_s|_{\max} = m|u_p|_{\max} = 3(2-\sqrt{3})mU_G \Big/ 4k. \tag{12}$$

Comparing the maximum value of $|u_s|$ with the minimum value of u_d, it is found that when turns ratio *m* is 6.96, the maximum value of $|u_s|$ is equal to the minimum value of u_d, which means the boundary turns ratio is 6.96. If the turns ratio *m* is less than 6.96, the ASFR does not work and the proposed rectifier operates as a conventional four-star 12-pulse diode rectifier. If the turns ratio *m* is more than 6.96, the ASFR works normally. Therefore, to ensure that the ASFR can work, the turns ratio *m* is greater than 6.96 in the proposed rectifier.

C. Operation Mode

In Fig. 1, the operation modes of the proposed 24-pulse diode rectifier are determined by the relation between the ASFR input voltage u_s and the load voltage u_d. According to the relation between u_s and u_d, the proposed 24-pulse diode rectifier has three operation modes: Z-mode, P-mode, and Q-mode. Fig. 3 shows the three operation modes.

1) Z-Mode: Whenever $|u_s| < u_d$, the proposed rectifier operates under Z-mode [see Fig. 3(a)]. In this mode, diodes D_p and D_q of the ASFR are reverse-biased and OFF, the currents i_p and i_q are zero, and the ASFR does not work. The proposed rectifier behaves as a conventional four-star 12-pulse diode rectifier. The currents i_{d5} and i_{d6} are

$$i_{d5} = i_{d6} = \frac{I_d}{2}. \tag{13}$$

2) P-Mode: Whenever $u_s > u_d$, the proposed rectifier operates under P-mode [see Fig. 3(b)]. In this mode, diode D_p of the ASFR is forward-biased and turned ON, i_p is positive $(i_p > 0)$, and it is injected to the load. Diode D_q of the ASFR is reverse-biased and OFF. The double-star diode rectifier I conducts and i_{d5} is positive $(i_{d5} > 0)$. The double-star diode rectifier II is reverse-biased and i_{d6} is zero. The MMF relationship of the MSSIPT for the P-mode is

$$i_{d5} \cdot \frac{N_p}{2} = i_p \cdot N_s \tag{14}$$

where N_p and N_s are the numbers of turns of the primary and half secondary windings of the MSSIPT, respectively.

In Fig. 3(b), according to Kirchhoff's current law, the relation among i_{d5}, i_p, i_f, and I_d is

$$i_{d5} + i_p = i_{d5} + i_f = I_d. \tag{15}$$

Substituting (2) and (14) into (15), (15) is transformed to

$$2mi_p + i_p = I_d. \tag{16}$$

From (14)–(16), the currents i_p, i_f, and i_{d5} are obtained as

$$\begin{cases} i_p = i_f = \dfrac{1}{2m+1} I_d \\ i_{d5} = \dfrac{2m}{2m+1} I_d. \end{cases} \tag{17}$$

3) Q-Mode: Whenever $-u_s > u_o$, the proposed rectifier operates under the Q-mode [see Fig. 3(c)]. In this mode, diode D_q of the ASFR is forward-biased and turned ON, i_q is positive $(i_q > 0)$, and it is injected to the load. Diode D_p of the ASFR is reverse-biased and OFF. The double-star diode rectifier II conducts and i_{d6} is positive $(i_{d6} > 0)$. The double-star diode rectifier I is reverse-biased and i_{d5} is zero. The MMF relationship of the MSSIPT for the Q-mode is

$$i_{d6} \cdot \frac{N_p}{2} = i_q \cdot N_s. \tag{18}$$

In Fig. 3(c), according to Kirchhoff's current law, the relation among i_{d6}, i_q, i_f, and I_d is

$$i_{d6} + i_q = i_{d6} + i_f = I_d. \tag{19}$$

Substituting (2) and (18) into (19), (19) is transformed to

$$2mi_q + i_q = I_d. \tag{20}$$

From (18)–(20), the currents i_q, i_f, and i_{d6} are obtained as

$$\begin{cases} i_q = i_f = \dfrac{1}{2m+1} I_d \\ i_{d6} = \dfrac{2m}{2m+1} I_d. \end{cases} \tag{21}$$

From the above analysis, it is noted that depending on the relation between the voltage u_s and u_d, the ASFR operates under different conduction modes and the ASFR input currents

i_p and i_q are shown in Fig. 4(a) and (b). Due to the ASFR, the currents i_{d5} and i_{d6} are modulated, as shown in Fig. 4(d) and (e). According to the relation among currents i_{d5} , i_{d6}, and i_A, the input line current i_A is shaped as well, and it obtains 24-pulse input line current under the optimal turns ratio, as shown in Fig. 4(f).

III. Optimal Turns Ratio, Current Rating, and Maximum Output Power of the ASFR

A. Optimal Turns Ratio

In this section, the input line current is analyzed and the optimal turns ratio of the MSSIPT is selected so that the input line current THD of the proposed rectifier is minimized.

In Fig. 1, according to the MMF equation of two double-star transformers, the input line current for phase "A" can be expressed in terms of three-phase half-wave rectifiers input currents as

$$i_A = \frac{1}{k}(i_{a1} - i_{a2} + i_{c2} - i_{c1} + \sqrt{3}i_{a3} - \sqrt{3}i_{a4}). \tag{22}$$

The input currents i_{a1}, i_{a2}, i_{a3}, i_{a4}, i_{c1}, and i_{c2} can be expressed in terms of three-phase half-wave rectifier output currents by switching functions as

$$\begin{cases} i_{a1} = i_{d1}S_{a1} = \dfrac{1}{2}i_{d5}S_{a1} \\ i_{a2} = i_{d2}S_{a2} = \dfrac{1}{2}i_{d5}S_{a2} \\ i_{a3} = i_{d3}S_{a3} = \dfrac{1}{2}i_{d6}S_{a3} \\ i_{a4} = i_{d4}S_{a4} = \dfrac{1}{2}i_{d6}S_{a4} \\ i_{c1} = i_{d1}S_{c1} = \dfrac{1}{2}i_{d5}S_{c1} \\ i_{c2} = i_{d2}S_{c2} = \dfrac{1}{2}i_{d5}S_{c2} \end{cases} \tag{23}$$

where S_{a1}, S_{a2}, S_{c1}, S_{c2}, S_{a3}, and S_{a4} are the switching functions. The switching function S_{a1} can be expressed as

$$S_{a1} = \begin{cases} 1, & 0 \le \omega t \le 2\pi/3 \\ 0, & 2\pi/3 \le \omega t \le 2\pi. \end{cases} \tag{24}$$

Under symmetrical system configuration, the relation among switching functions is as follows:

$$\begin{cases} S_{a2} = S_{a1}\angle\text{-}\pi \\ S_{c1} = S_{a1}\angle\dfrac{2\pi}{3} \\ S_{c2} = S_{a1}\angle -\dfrac{\pi}{3} \\ S_{a3} = S_{a1}\angle -\dfrac{\pi}{6} \\ S_{a4} = S_{a1}\angle\dfrac{5\pi}{6}. \end{cases} \tag{25}$$

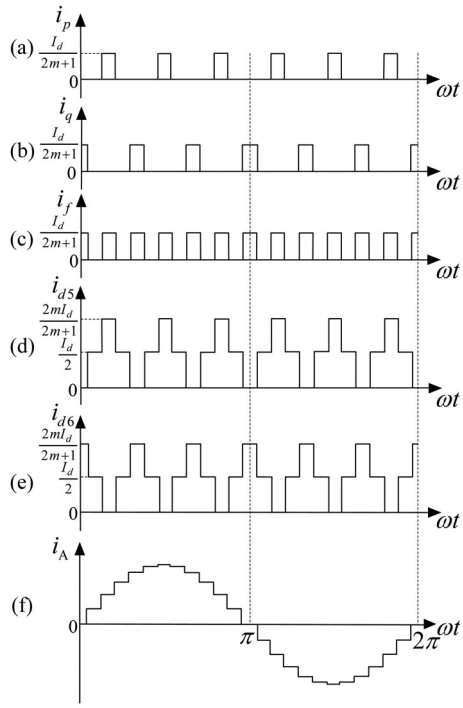

Fig. 4. Currents waves of the proposed rectifier under optimal turns ratio. (a) ASFR input current i_p. (b) ASFR input current i_q. (c) ASFR output current i_f. (d) Current i_{d5} . (e) Current i_{d6}. (f) Input line current i_A.

Substituting (23) into (22), we obtain

$$\begin{aligned} i_A &= \frac{1}{k}[(S_{a1}-S_{c1})i_{d1}+(S_{c2}-S_{a2})i_{d2}+\sqrt{3}S_{a3}i_{d3}-\sqrt{3}S_{a4}i_{d4}) \\ &= \frac{1}{2k}[i_{d5}(S_{a1}-S_{a2}+S_{c2}-S_{c1})+i_{d6}(\sqrt{3}S_{a3}-\sqrt{3}S_{a4})]. \end{aligned} \tag{26}$$

In the above expression, it is noted that the input line current i_A is dependent on the currents i_{d5} and i_{d6}. To obtain the expression of the input line current i_A, expressions of currents i_{d5} and i_{d6} should be obtained first.

Fig. 4(d) and (e) shows the currents i_{d5} and i_{d6}. To express the waveforms of currents i_{d5} and i_{d6} in a mathematical form, phase angles when the ASFR changes its conduction mode are vital. At these phase angles, the ASFR input voltage $|u_s|$ is equal to the load voltage u_d. For $\omega t > 0$, the first phase angle when input voltage $|u_s|$ is equal to load voltage u_d is defined as ϕ, and it meets

$$u_d(\phi) = |u_s(\phi)| = m\,|u_p(\phi)|\,. \tag{27}$$

Since the voltage $|u_p|$ is symmetrical and its period is one-twelfth of input phase voltage, the phase angle ϕ is located in

$$0 \le \phi \le \frac{\pi}{12}. \tag{28}$$

Substituting (10) and (11) into (27), the resulting equation is

$$\begin{aligned} \frac{3(\sqrt{6}+\sqrt{2})U_G}{8k}\sin(\phi+5\pi/12) &= \frac{3m(\sqrt{6}-\sqrt{2})U_G}{4k} \\ &\quad\times\cos(\phi+5\pi/12). \end{aligned} \tag{29}$$

Solving the above equation, the phase angle ϕ is

$$\phi = \arctan\left(\frac{2m(\sqrt{6}-\sqrt{2})}{\sqrt{6}+\sqrt{2}}\right) - 5\pi/12. \tag{30}$$

Utilizing the periodicity and symmetry of the input voltage $|u_s|$ and load voltage u_d, other phase angles where the ASFR conduction modes change can be expressed easily as functions of ϕ.

Combining Fig. 4(d) and (e), the currents i_{d5} and i_{d6} are expressed as

$$id_5 = \begin{cases} 0, & \omega t \in \left[\frac{\pi}{3}p, \frac{\pi}{3}p+\phi\right] \\ \frac{I_d}{2}, & \omega t \in \left[\frac{\pi}{3}p+\phi, \frac{\pi}{3}p+\frac{\pi}{6}-\phi\right] \\ \frac{2mI_d}{2m+1}, & \omega t \in \left[\frac{\pi}{3}p+\frac{\pi}{6}-\phi, \frac{\pi}{3}p+\frac{\pi}{6}+\phi\right] \\ \frac{I_d}{2}, & \omega t \in \left[\frac{\pi}{3}p+\frac{\pi}{6}+\phi, \frac{\pi}{3}p+\frac{\pi}{3}-\phi\right] \\ 0, & \omega t \in \left[\frac{\pi}{3}p+\frac{\pi}{3}-\phi, \frac{\pi}{3}p+\frac{\pi}{3}\right] \end{cases} \tag{31}$$

$$id_6 = \begin{cases} \frac{2mI_d}{2m+1}, & \omega t \in \left[\frac{\pi}{3}p, \frac{\pi}{3}p+\phi\right] \\ \frac{I_d}{2}, & \omega t \in \left[\frac{\pi}{3}p+\phi, \frac{\pi}{3}p+\frac{\pi}{6}-\phi\right] \\ 0, & \omega t \in \left[\frac{\pi}{3}p+\frac{\pi}{6}-\phi, \frac{\pi}{3}p+\frac{\pi}{6}+\phi\right] \\ \frac{I_d}{2}, & \omega t \in \left[\frac{\pi}{3}p+\frac{\pi}{6}+\phi, \frac{\pi}{3}p+\frac{\pi}{3}-\phi\right] \\ \frac{2mI_d}{2m+1}, & \omega t \in \left[\frac{\pi}{3}p+\frac{\pi}{3}-\phi, \frac{\pi}{3}p+\frac{\pi}{3}\right] \end{cases} \tag{32}$$

where $p = 0, 1, 2, 3, 4, 5$.

In the interval $\omega t \in [0, \pi/2]$, substituting (31) and (32) into (26), the expression of input line current i_A is obtained as

$$i_A = \begin{cases} 0, & \omega t \in [0, \phi] \\ \frac{I_d}{4k}, & \omega t \in \left[\phi, \frac{\pi}{6}-\phi\right] \\ \frac{mI_d}{k(2m+1)}, & \omega t \in \left[\frac{\pi}{6}-\phi, \frac{\pi}{6}+\phi\right] \\ \frac{I_d}{4k}(1+\sqrt{3}), & \omega t \in \left[\frac{\pi}{6}+\phi, \frac{\pi}{3}-\phi\right] \\ \frac{\sqrt{3}mI_d}{k(2m+1)}, & \omega t \in \left[\frac{\pi}{3}-\phi, \frac{\pi}{3}+\phi\right] \\ I_d\left(\frac{1}{2k}+\frac{\sqrt{3}}{4k}\right), & \omega t \in \left[\frac{\pi}{3}+\phi, \frac{\pi}{2}-\phi\right] \\ \frac{2mI_d}{k(2m+1)}, & \omega t \in \left[\frac{\pi}{2}-\phi, \frac{\pi}{2}\right]. \end{cases} \tag{33}$$

The interval $\omega t \in [0, \pi/2]$ is chosen since it is sufficient to determine the input line current THD. In (33), it is clear that the input line current i_A is dependent on the turns ratio m. Fig. 5 shows the variation in THD of i_A for different turns ratio m.

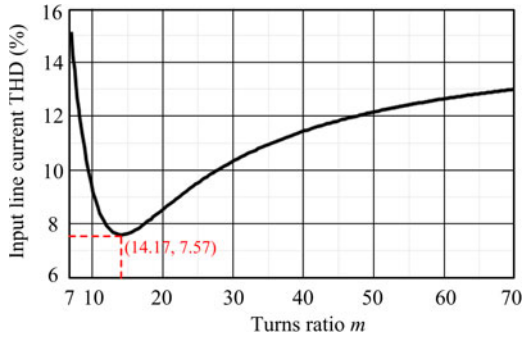

Fig. 5. Variation in THD of i_A for different turns ratio m.

In Fig. 5, the minimum THD of i_A is shown to be 7.57%, which is the same as achieved by classical 24-pulse rectifiers, at turns ratio $m = m_{\text{opt}} = 14.7$. Under the optimal turns ratio $m_{\text{opt}} = 14.17$, the phase angle ϕ is obtained as

$$\phi = \arctan\left(\frac{2m(\sqrt{6}-\sqrt{2})}{\sqrt{6}+\sqrt{2}}\right) - 5\pi/12\Big|_{m_{\text{opt}}} = \frac{\pi}{24}. \tag{34}$$

Under the optimal turns ratio, the Fourier series expansion of the input line current i_A is calculated as

$$i_A = \sum_{n=\text{odd}}^{\infty} \frac{B_n I_d}{2kn\pi(2\sqrt{3}+\sqrt{2}+2+2\sqrt{2})} \sin(n\omega t) \tag{35}$$

where

$$\begin{aligned} B_n = {} & (2+2\sqrt{2}+2\sqrt{3}+\sqrt{6})\left(\cos\left(\frac{n\pi}{24}\right) - \cos\left(\frac{23n\pi}{24}\right)\right) \\ & +(3+2\sqrt{2}+\sqrt{3}+\sqrt{6})\left(\cos\left(\frac{3n\pi}{24}\right) - \cos\left(\frac{21n\pi}{24}\right)\right) \\ & +(\sqrt{2}+\sqrt{3}+3+\sqrt{6})\left(\cos\left(\frac{5n\pi}{24}\right) - \cos\left(\frac{19n\pi}{24}\right)\right) \\ & +(1+\sqrt{2}+\sqrt{3}+\sqrt{6})\left(\cos\left(\frac{7n\pi}{24}\right) - \cos\left(\frac{17n\pi}{24}\right)\right) \\ & +(1+\sqrt{2}+\sqrt{3})\left(\cos\left(\frac{9n\pi}{24}\right) - \cos\left(\frac{15n\pi}{24}\right)\right) \\ & +\sqrt{2}\left(\cos\left(\frac{11n\pi}{24}\right) - \cos\left(\frac{13n\pi}{24}\right)\right) \end{aligned} \tag{36}$$

In (36), only when $n = 24h \pm 1(\text{h} : \text{integer})$, it is not zero. For other odd numbers, it is zero. It means that the input line current of the proposed rectifier only includes $(24h \pm 1)$ th harmonics. The proposed rectifier behaves as a 24-pulse rectifier under the optimal turns ratio $m_{opt} = 14.17$. Fig. 4(f) illustrates the input line current i_A under the optimal turns ratio.

B. Current Rating of the ASFR

In this section, the currents i_p and i_q are obtained first; then, the current rating and total diode conduction losses are analyzed.

Under the optimal turns ratio $m_{\rm opt} = 14.17$, the currents i_p and i_q shown in Fig. 4(a) and (b) can be expressed as

$$i_p = \begin{cases} 0, & \omega t \in \left[\frac{\pi}{3}p, \frac{\pi}{3}p + \frac{\pi}{8}\right] \\ \frac{I_d}{2 \times 14.17 + 1}, & \omega t \in \left[\frac{\pi}{3}p + \frac{\pi}{8}, \frac{\pi}{3}p + \frac{5\pi}{24}\right] \\ 0, & \omega t \in \left[\frac{\pi}{3}p + \frac{5\pi}{24}, \frac{\pi}{3}p + \frac{\pi}{3}\right] \end{cases} \quad (37)$$

$$i_q = \begin{cases} \frac{I_d}{2 \times 14.17 + 1}, & \omega t \in \left[\frac{\pi}{3}p, \frac{\pi}{3}p + \frac{\pi}{24}\right] \\ 0, & \omega t \in \left[\frac{\pi}{3}p + \frac{\pi}{24}, \frac{\pi}{3}p + \frac{7\pi}{24}\right] \\ \frac{I_d}{2 \times 14.17 + 1}, & \omega t \in \left[\frac{\pi}{3}p + \frac{7\pi}{24}, \frac{\pi}{3}p + \frac{\pi}{3}\right] \end{cases} \quad (38)$$

where $p = 0, 1, 2, 3, 4, 5$.

In Fig. 1, according to Kirchhoff's current law, the ASFR output current i_f is obtained as

$$i_f = i_p + i_q. \quad (39)$$

Substituting (37) and (38) into (39), the current i_f is

$$i_f = \begin{cases} \frac{I_d}{2 \times 14.17 + 1}, & \omega t \in \left[\frac{\pi}{3}p, \frac{\pi}{3}p + \frac{\pi}{24}\right] \\ 0, & \omega t \in \left[\frac{\pi}{3}p + \frac{\pi}{24}, \frac{\pi}{3}p + \frac{\pi}{8}\right] \\ \frac{I_d}{2 \times 14.17 + 1}, & \omega t \in \left[\frac{\pi}{3}p + \frac{\pi}{8}, \frac{\pi}{3}p + \frac{5\pi}{24}\right] \\ 0, & \omega t \in \left[\frac{\pi}{3}p + \frac{5\pi}{24}, \frac{\pi}{3}p + \frac{7\pi}{24}\right] \\ \frac{I_d}{2 \times 14.17 + 1}, & \omega t \in \left[\frac{\pi}{3}p + \frac{7\pi}{24}, \frac{\pi}{3}p + \frac{\pi}{3}\right] \end{cases} \quad (40)$$

where $p = 0, 1, 2, 3, 4, 5$.

From (40), the maximum current through the ASFR is obtained as

$$i_{f\,\max} = \frac{I_d}{2 \times 14.17 + 1} = 3.4\% I_d. \quad (41)$$

The average current through the ASFR is calculated as

$$I_{\text{Av-asfr}} = \frac{1}{2\pi} \int_0^{2\pi} i_f d\omega t = 1.7\% I_d. \quad (42)$$

In Fig. 1, the ASFR consists of two additional diodes D_p and D_q; it means that the total average current through two additional diodes D_p and D_q is 1.7% of the load current. Compared with the 24-pulse rectifiers with TIPT [16]–[20], the total average current through the two additional diodes is observably reduced from $100\%\, I_d$ to $1.7\%\ I_d$,which means the conduction losses of the two additional diodes is sharply reduced by the proposed method.

TABLE I
SYSTEM SPECIFICATIONS AND COMPONENTS FOR EXPERIMENT

PARAMETER	VALUE
Input line-to-line voltage (rms)	380 V
Line frequency	50 Hz
Double-star transformer turn ratio (Δ/*Y*/*Y*)	8.2:1:1
Double-star transformer turn ratio (*Y*/*Y*/*Y*)	4.7:1:1
Leakage inductances of double-star transformer	0.15 mH
Load filtering inductance	15 mH
Turns ratio of the MSSIPT	1:14.2:14.2
Rated output power	1 kW
Rated output current	18 A
The ASFR	1 N 4004 × 2

To compare the total diodes conduction losses, the respective losses for the 24-pulse rectifier with TIPT [16]–[20] and the proposed 24-pulse rectifier are given by (43) and (44), respectively:

$$\begin{aligned} P_{\text{loss-TIPT}} &= 12 \cdot I_{D\text{av}} \cdot 2 \cdot V_{\text{on}} + I_d \cdot V_{\text{on-add}} \\ &= 12 \cdot \frac{I_d}{12} \cdot 2 \cdot V_{\text{on}} + I_d \cdot V_{\text{on-add}} \\ &= I_d(2V_{\text{on}} + V_{\text{on-add}}). \end{aligned} \quad (43)$$

$$\begin{aligned} P_{\text{loss-proposed}} &= 12 \cdot I_{D\text{av}} \cdot V_{\text{on}} + I_{\text{add-av}} V_{\text{on-add}} \\ &= 12 \cdot \frac{I_d}{12} \cdot V_{\text{on}} + 0.017 I_d V_{\text{on-add}} \\ &= I_d(V_{\text{on}} + 0.017 V_{\text{on-add}}). \end{aligned} \quad (44)$$

In the above expressions, I_d is the load current, $I_{D\text{av}}$ is the average current through the diodes of the main circuit, and V_{on} is the forward voltage drop of the diodes of the main circuit. $I_{\text{add-av}}$ is the average current through the additional diodes and $V_{\text{on-add}}$ is the forward voltage-drop of the additional diodes.

From (43) and (44), it is noted that compared with the 24-pulse rectifiers with TIPT [16]–[20], the total diode conduction losses are reduced effectively. The proposed rectifier is more suitable for low-voltage and high-current applications.

C. Maximum Output Power of the ASFR

When the output current i_f is the maximum value, the output power of the ASFR is maximum. Combining (42), the maximum output power of ASFR is expressed as

$$p_{\text{masfr}} = \frac{I_d}{2 \times 14.17 + 1} u_d = 3.4\% p_d \quad (45)$$

where $p_d = I_d u_d$ is the output power of the proposed rectifier.

In (45), it is clear that the maximum output power of ASFR is only 3.4% the rectifier system output power; the proposed scheme is suitable for high-power applications.

IV. EXPERIMENT RESULTS

An experimental setup with 1 kW is built to verify the theoretical analysis and function of the ASFR. Table I shows the system specifications and components for experiment.

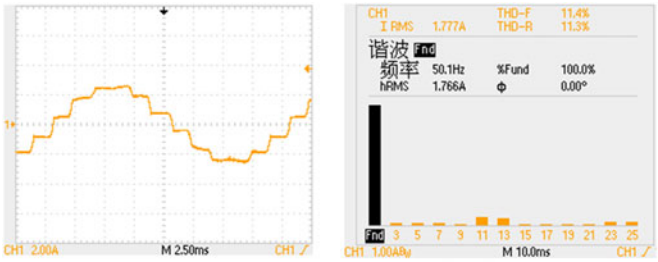

Fig. 6. Measured waveforms without ASFR. (a) Input line current i_A. (b) Spectrum of i_A.

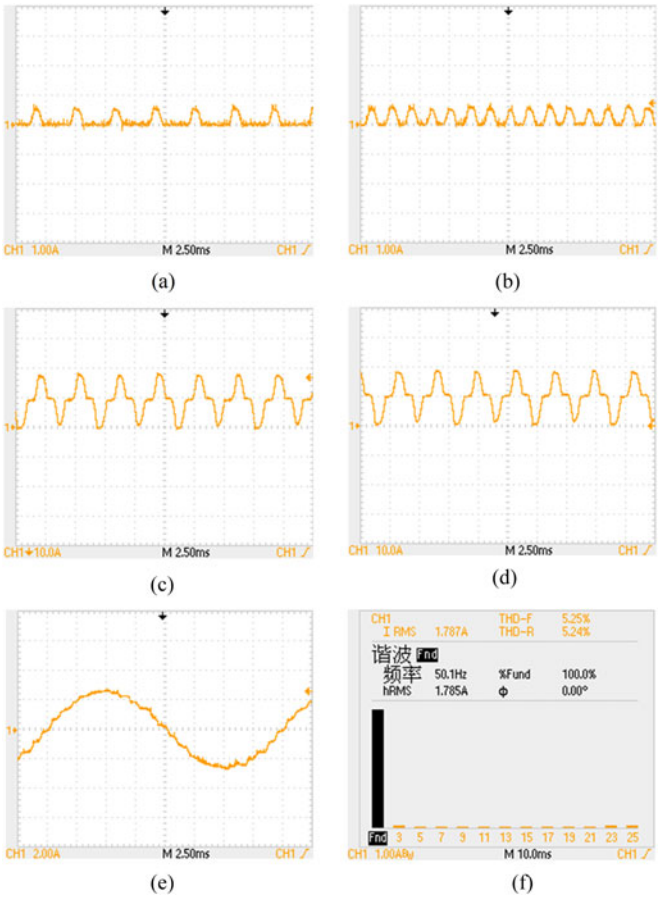

Fig. 7. Measured waveforms for the proposed rectifier. (a) ASFR input current i_p. (b) ASFR output current i_f. (c) Double-star rectifier I output current i_{d5}. (d) Double-star rectifier II output current i_{d6}. (e) Input line current i_A. (f) Spectrum of i_A.

Under the rated conditions listed in Table I, Figs. 6 and 7 show the measured waveforms without and with the ASFR.

If the ASFR is not used, the proposed rectifier behaves as a conventional four-star 12-pulse rectifier; the input line current i_A and its spectrum are shown in Fig. 6.

In Fig. 6, the input line current THD is 11.4%, which is slightly less than the theoretical values 15.2% due to the leakage inductances of double-star transformer.

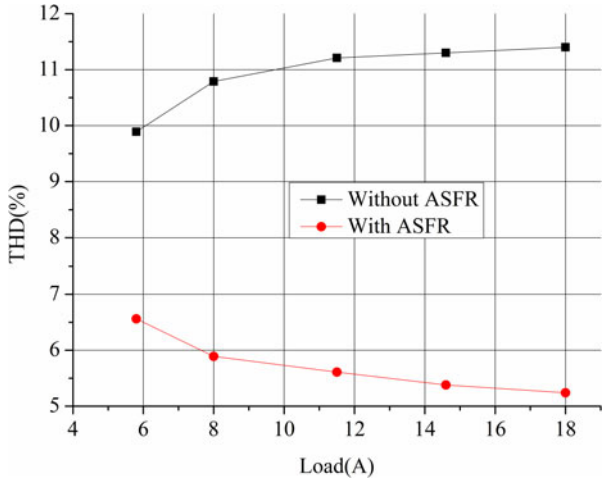

Fig. 8. Comparison of THD without and with ASFR.

When the ASFR is used, the proposed rectifier behaves as a 24-pulse rectifier. Fig. 7 shows the measured waveforms. Fig. 7(a) and (b) shows the ASFR input currents i_p and the ASFR output currents i_f, respectively. The maximum value of the current i_p is 0.6 A and the average value of the current i_f is 0.29 A. The maximum value of the current i_p and the average value of the current i_f are 3.3% and 1.6%, respectively, of load current (18 A), which are slightly less than the theoretical values (3.4% and of 1.7%) due to the leakage inductances of double-star transformer. Fig. 7(c) and (d) shows the currents i_{d5} and i_{d6}; the waveforms of currents i_{d5} and i_{d6} basically coincide with the theoretical analysis in Fig. 4(d) and (e). Fig. 7(e) and (f) shows the input line current i_A and its spectrum. Compared with Fig. 6(a) and (b), it is obvious that the ASFR is effective on reducing harmonic distortion of the rectifier input currents. The input line current THD decreases from 11.4% to 5.25%, and the 5th, 7th, 11th, 13th, 17th, and 19th harmonics are eliminated.

Under different load conditions, Fig. 8 compares the input line current THD without and with ASFR.

In Fig. 8, it is clear that owing to the ASFR, the input line current THD is reduced effectively.

V. Conclusion

This paper proposed an ASFR scheme to extend the conventional four-star 12-pulse operation to 24-pulse operation. The low-power (3.4%Po) ASFR is connected with the additional winding of the MSSIPT, and it extracts two rectangular currents from the MSSIPT to shape the output current of two double-star rectifiers first, which in turn double the pulse of the input line currents. The resulting 24-pulse rectifier draws near sinusoidal input line currents with the absence of 5th, 7th, 11th, 13th, 17th, and 19th harmonics. The operation mode of the proposed rectifier is analyzed and the optimal turns ratio of MSSIPT is derived in this paper. Under the optimal turns ratio, the current through the ASFR has maximum and average values of 3.4% and 1.7%, respectively, of the load current, which means that the current

rating and conduction losses of the ASFR are very low. The proposed 24-pulse diode rectifier has low-diode conduction losses, and it is suitable for high-current applications. Since only a low-power (3.4% Po) ASFR is enough, the proposed method is low cost, robust, and simple to implement.

REFERENCES

[1] B. Singh, S. Gairola, B. N. Singh, A. Chandra, and K. Al-Haddad, "Multipulse AC-DC converters for improving power quality: A review," *IEEE Trans. Power Electron.*, vol. 23, no. 1, pp. 260–281, Jan. 2008.

[2] J. R. Rodriguez *et al.*, "Large current rectifiers: State of the art and future trends," *IEEE Trans. Ind. Electron.*, vol. 52, no. 3, pp. 738–746, Jun. 2005.

[3] J. Das, *Harmonic Reduction at the Source*. New York, NY, USA: IEEE Press, 2015.

[4] L. Wei, N. N. Guskov, R. A. Richard, and G. L. Skibinski, "Mitigation of current harmonics for multipulse diode front-end rectifier systems," *IEEE Trans. Ind. Appl.*, vol. 43, no. 3, pp.787–797, May 2007.

[5] C. Young, S. Wu, W. Yeh, and C. Yeh, "A dc-side current injection method for improving AC line condition applied in the 18-pulse converter system," *IEEE Trans. Power Electron.*, vol. 29, no. 1, pp. 99–109, Jan. 2014.

[6] S. Choi, P. N. Enjeti, H. H. Lee, and I. J. Pitel, "A new active inter-phase reactor for 12-pulse rectifiers provides clean power utility interface," *IEEE Trans. Ind. Appl.*, vol. 32, no. 6, pp. 1304–1311, Nov./Dec. 1996.

[7] H. Akagi and K. Isozaki, "A hybrid active filter for a three-phase 12-pulse diode rectifier used as the front end of a medium-voltage motor drive," *IEEE Trans. Power Electron.*, vol. 27, no. 1, pp. 69–77, Jan. 2012.

[8] T. H. Nguyen, D. C. Lee, and C. K. Kim, "A series-connected topology of a diode rectifier and a voltage-source converter for an HVDC transmission system," *IEEE Trans. Power Electron.*, vol. 29, no. 4, pp. 1579–1584, Apr. 2014.

[9] B. Singh, G. Bhuvaneswari, and V. Garg, "T-connected autotransformer-based 24-pulse AC–DC converter for variable frequency induction motor drive," *IEEE Trans. Energy Convers.*, vol. 21, no. 3, pp. 663–672, Sep. 2006.

[10] E. Wiechmann, R. Burgos, and J. Rodriguez, "High power factor phase controlled rectifier using staggered converters," in *Proc. Conf. Rec. IEEE Ind. Appl. Conf.*, Oct. 5–9, 1997, pp. 1390–1397.

[11] C. Guimaraes, G. Olivier, and G. E. April, "High current ac/dc power converters using T-connected transformers," in *Proc. IEEE Can. Conf. Elect. Comput. Eng.*, Sep. 5–8, 1995, pp. 704–707.

[12] Y. Wenli *et al.*, "Zero sequence blocking transformers for multi-pulse rectifier in aerospace applications," in *Proc. IEEE Energy Convers. Congr. Expo.*, Sep. 14–18, 2014, pp. 999–1006.

[13] P. Bozovic and P. Pejovic, "Current-injection-based 12-pulse rectifier using a single three-phase diode bridge," *IET Electr. Power Appl.*, vol. 1, no. 2, pp. 209–216, Mar. 2007.

[14] J. Arrillaga and M. E. Villablanca, "Pulse doubling in parallel convertor configurations with interphase reactors," *IEE Proc.—Electr. Power Appl.*, vol. 138, no. 1, pp. 15–20, Jan. 1991.

[15] S. Miyairi, S. Iida, K. Nakata, and S. Masukawa, "New method for reducing harmonics involved in input and output of rectifier with interphase transformer," *IEEE Trans. Ind. Appl.*, vol. IA-22, no. 5, pp. 790–797, Sep./Oct. 1986.

[16] S. Choi, B. S. Lee, and P. N. Enjeti, "New 24-pulse diode rectifier systems for utility interface of high power AC motor drives," *IEEE Trans. Ind. Appl.*, vol. 33, no. 2, pp. 531–541, Mar./Apr. 1997.

[17] M, Kang, B. O. Woo, P. Enjeti, and I. J. Pitel, "Autoconnected-electronic-transformer-based multipulse rectifiers for utility interface of power electronic systems," *IEEE Trans. Ind. Appl.*, vol. IA-35, no. 3, pp. 646–656, May 1999.

[18] B. Singh, V. Garg, and G. Bhuvaneswari, "Polygon-connected autotransformer-based 24-pulse AC–DC converter for vector-controlled induction-motor drives," *IEEE Trans. Ind. Electron.*, vol. 55, no. 1, pp. 197–208, Jan. 2008.

[19] Q. Pan, W. Ma, and D. Liu, "A new critical formula and mathematical model of double-tap interphase reactor in a six-phase tap-changer diode rectifier," *IEEE Trans. Ind. Electron.*, vol. 54, no. 1, pp. 479–485, Feb. 2007.

[20] F. Meng, S. Yang, and W. Yang, "Modeling for a multitap interphase reactor in a multipulse diode bridge rectifier," *IEEE Trans. Power Electron.*, vol. 24, no. 9, pp. 2171–2177, Sep. 2009.

Shiyan Yang was born in Heilongjiang, China, in 1962. He received the B.S. and M.S. degrees in electrical engineering and the Ph.D. degree in welding engineering from the Harbin Institute of Technology, Harbin, China, in 1984, 1989, and 1998, respectively.

He is currently a Professor and Supervisor for Doctoral Candidates with the Harbin Institute of Technology. He has published more than 60 papers. His research interests include high-power special type power supply and its application, energy storage system and its equilibrium, and fundamental theory of finity power supply drive and key commonsense problem.

Jingfang Wang was born in Hebei, China, in 1984. He received the B.S. degree in Automation from Yanshan University, Qinhuangdao, China, in 2008, and the M.S. degree in electrical engineering from the Harbin Engineering University, Harbin, China, in 2012. Since 2012, he has been working toward the Ph.D. degree in electrical engineering from the Harbin Institute of Technology, Harbin, China.

His research interests include high power converters and harmonics compensation.

Wei Yang (M'09) was born in Heilongjiang, China, in 1978. He received the B.S., M.S., and Ph.D. degrees in electrical engineering from the Harbin Institute of Technology, Harbin, China, in 2001, 2005, and 2010, respectively.

His research interests include power electronics and motor drives.